Stabilization of Fe−Pd Nanoparticles with Sodium Carboxymethyl Cellulose for Enhanced Transport and Dechlorination of Trichloroethylene in Soil and Groundwater

ARTICLE *in* INDUSTRIAL & ENGINEERING CHEMISTRY RESEARCH · NOVEMBER 2006

Impact Factor: 2.59 · DOI: 10.1021/ie0610896

4 AUTHORS, INCLUDING:

Feng he
Zhejiang University of Technology
27 PUBLICATIONS **1,572** CITATIONS
SEE PROFILE

Dongye Zhao
Auburn University
114 PUBLICATIONS **3,363** CITATIONS
SEE PROFILE

Juncheng Liu
Alto Products Corporation
47 PUBLICATIONS **1,469** CITATIONS
SEE PROFILE

Stabilization of Fe−Pd Nanoparticles with Sodium Carboxymethyl Cellulose for Enhanced Transport and Dechlorination of Trichloroethylene in Soil and Groundwater

Feng He,[†] Dongye Zhao,*[,†] Juncheng Liu,[‡] and Christopher B. Roberts[‡]

Department of Civil Engineering, Environmental Engineering Program, and Department of Chemical Engineering, Auburn University, Auburn, Alabama 36849

This study reports a new strategy for stabilizing palladized iron (Fe−Pd) nanoparticles with sodium carboxymethyl cellulose (CMC) as a stabilizer. Compared to nonstabilized Fe−Pd particles, the CMC-stabilized nanoparticles displayed markedly improved stability against aggregation, chemical reactivity, and soil transport. Transmission electron microscopy (TEM) and dynamic light scattering (DLS) analyses indicated that the CMC-stabilized nanoparticles with a diameter <17.2 nm are highly dispersed in water. Fourier transform infrared (FTIR) spectroscopy results suggested that CMC molecules were adsorbed to iron nanoparticles primarily through the carboxylate groups through monodentate complexation. In addition, −OH groups in CMC were also involved in interactions with iron particles. Batch dechlorination tests demonstrated that the CMC-stabilized nanoparticles degraded trichloroethene (TCE) 17 times faster than their nonstabilized counterparts based on the initial pseudo-first-order rate constant. Last, column tests showed that the stabilized nanoparticles can be readily transported in a loamy-sand soil and then eluted completely with three bed volumes of deionized (DI) water.

Introduction

In situ dechlorination by direct injection of zerovalent iron (ZVI) nanoparticles into the contaminated subsurface has attracted increasing interest in recent years.[1−3] Compared to the traditional passive processes such as the "funnel and gate" or permeable reactive barrier (PRB) processes, the in situ injection technology offers a number of key advantages.[2] For example, it can proactively attack contaminant plumes in the source zone and potentially reduce the remediation cost and time substantially.[2]

However, this promising technology has been held back by the key technical barrier that the nanoparticles tend to agglomerate and grow to micron scale or larger, thereby rapidly losing their soil mobility and chemical reactivity.[4−6] Typically, Fe(0)-based nanoparticles are prepared by reducing Fe(II) or Fe(III) in an aqueous phase using sodium borohydride.[1,7] Although other solvent-based methods such as microemulsion-based methods,[8] sonication-assisted methods,[9,10] and sol−gel methods[11] have been reported, the water-based approach appears most suitable for environmental applications because of its minimal use of environmentally harmful solvents or chemicals. However, because of particle agglomeration, the water-based method often fails to produce the desired stable Fe nanoparticles without a stabilizer.

Agglomeration of magnetic metal nanoparticles takes place primarily through direct interparticle interactions such as van der Waals forces and magnetic interactions.[12] Agglomeration reduces the specific surface area and the interfacial free energy, thereby diminishing particle reactivity. A stabilizer can enhance dispersion (or reduce agglomeration) of nanoparticles through (a) electrostatic repulsion (i.e., adsorption of charged stabilizer molecules to the metal core results in an enhanced electrical double layer and, thus, increased Coulombic repulsion between the capped particles) and (b) steric hindrance (i.e., coating the metal core with sterically bulky stabilizers such as polymers impedes particle attractions).[12] In addition to weakening the physical interactions, encapsulating nanoparticles with select stabilizers can also passivate the highly reactive surface from reacting with the surrounding media such as dissolved oxygen (DO) and water. Although the surface passivating effect might also inhibit reaction with target contaminants, the net reactivity gain toward a target compound can be substantial because of the tremendous particle size reduction and the gain in surface area from the particle stabilization.

Extensive studies have been devoted to stabilizing non-ZVI (e.g., gold, silver, and iron oxide) nanoparticles. For instance, to prevent nanoscale iron oxides from agglomeration, various stabilizers have been found to be effective, including thiols,[13] carboxylic acids,[14] surfactants,[15] and polymers.[16−18] Obviously, not all of these stabilizers are applicable to the ZVI nanoparticles of interest. For example, thiols and carboxylic acids can be reduced by ZVI, some polymers might not function properly in water,[19] some stabilizers themselves are not environmentally benign, and others are cost-prohibitive. However, the fundamentals and experimental approaches gained from these studies provide a valuable knowledge base for studying the stabilization of ZVI nanoparticles.

In contrast, only limited studies have been reported on stabilizing ZVI nanoparticles. Mallouk et al. employed carbon nanoparticles and poly(acrylic acid) (PAA) as "vehicles" for stabilizing and/or delivering Fe-based nanoparticles.[5,20,21] Saleh et al. proposed a new type of sorptive nanoparticles prepared by modifying commercial ZVI nanoparticles with so-called "block copolymer shells" consisting of a hydrophobic inner shell and a hydrophilic outer shell for dechlorination of dense nonaqueous-phase liquids (DNAPLs).[22] Sun and Zhang reported that using polyvinyl alcohols can reduce the size of the Fe nanoparticles (or their aggregates) from 60 to 7.9 nm.[23]

* To whom correspondence should be addressed. Tel.: (334)844-6277. Fax: (334)844-6290. E-mail: dzhao@eng.auburn.edu.

[†] Department of Civil Engineering, Environmental Engineering Program.

[‡] Department of Chemical Engineering.

10.1021/ie0610896 CCC: $37.00
Published on Web 11/29/2006

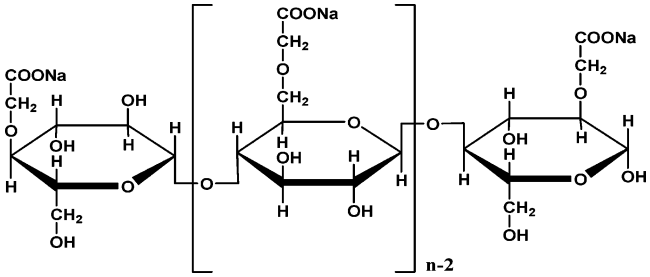

Figure 1. Conceptualized representation of the molecular structure of NaCMC.

To implement the in situ injection of Fe nanoparticles, an ideal stabilizer should (a) be able to specifically interact with the nanoparticles and hence suppress their growth, (b) be environmentally benign, (c) be cost-effective, and (d) be mobile in soils. Recently, He and Zhao reported that a food-grade water-soluble starch can improve both the dispersibility and the reactivity of Fe nanoparticles.[6] Unfortunately, the starched Fe particles became less stable, as evidenced by the appearance of floc precipitates after 2 days, thereby limiting long-term storage and commercial application of these Fe nanoparticles. A better stabilizer with stronger interactions with the Fe particles needs to be developed that will allow longer-lasting effective stabilization and facilitate environmental applications of these nanoparticles.

Cellulose is a carbohydrate consisting of a series of hydroglucose units interconnected by an oxygen linkage (known as a beta linkage) to form a linear molecular chain structure. Cellulose can easily be modified to sodium carboxymethyl cellulose (CMC) by replacing the native CH_2OH group in the glucose unit with a carboxymethyl group. Figure 1 presents a conceptualized representation of the molecular structure of CMC. CMC is water-soluble and is commonly used in food processing.[24] CMC has been successfully used as an effective stabilizer in preparing nanoparticles such as superparamagnetic iron oxide nanoparticles (SPIONs) and Ag nanoparticles.[17,25] Like starch, CMC is also low-cost and environmentally friendly. CMC and starch share similar macromolecular skeletons. However, CMC is a polyelectrolyte and carries carboxylate groups in addition to hydroxyl groups. Consequently, CMC is expected to interact with Fe nanoparticles more strongly and stabilize the nanoparticles more effectively.

This work aimed to investigate the feasibility of using CMC as a novel stabilizer for preparing physically more stable and chemically more reactive Fe−Pd nanoparticles for the degradation of trichloroethene (TCE) in soils and water. The specific objectives were to (1) prepare a new class of Fe−Pd nanoparticles using CMC as a stabilizer, (2) elucidate the mechanisms governing the particle stabilization, (3) probe the dechlorination reactivity of the nanoparticles with TCE as a model chlorinated hydrocarbon, and (4) preliminarily test the mobility of the CMC-stabilized iron particles in soil.

Experimental Section

Chemicals. The following chemicals were used as received: TCE (>99%, spectrophotometric grade, Aldrich, Milwaukee, WI), hexane (pesticide grade, Fisher Scientific, Fair Lawn, NJ), K_2PdCl_6 (99%, Acros Organics, Morris Plains, NJ), $FeSO_4 \cdot 7H_2O$ (Acros Organics), sodium carboxymethyl cellulose (NaCMC or CMC, mean MW = 90 000, Acros Organics), and sodium borohydride ($NaBH_4$, ICN Biomedicals, Aurora, OH).

Preparation of Nanoparticles. Fe−Pd nanoparticles were prepared by modifying a water-based approach[6] with two changes: (a) CMC was used as a stabilizer, and (b) $FeSO_4 \cdot 7H_2O$ was used as the starting salt for the ZVI nanoparticles. Compared to the commonly used $FeCl_3$, $FeSO_4 \cdot 7H_2O$ offers several advantages: (a) it allows for monitoring chloride production during the dechlorination reaction; (b) ferrous ions form stable complexes with CMC, whereas ferric ions can induce flocculation of CMC; and (c) reduction of ferrous ions consumes less borohydride. In brief, the preparation was carried out in a 250-mL flask attached to a vacuum line. Before use, deionized (DI) water and the CMC solution were purged with purified N_2 for 15 min to remove DO. In a typical preparation, a stock solution of 0.21 M $FeSO_4 \cdot 7H_2O$ was prepared right before use and then was added to the CMC solution through a burette to yield the desired concentration of Fe and CMC. The mixture was purged with N_2 for 15 min to complete the formation of the Fe−CMC complex. The Fe concentration used in this study was 0.1 or 1 g/L, and the corresponding CMC (in sodium form) concentration was 0.2% or 0.8% (w/w).

The Fe^{2+} ions were then reduced to Fe^0 by adding a certain amount of sodium borohydride ($BH_4^-/Fe^{2+} = 2.0$) to the mixture. To ensure efficient use of the reducing agent BH_4^-, the reactor system was operated under inert conditions through continuous vacuuming. The flask was shaken by hand during the reaction. When gas (hydrogen) evolution ceased (after ~15 min), the Fe^0 nanoparticles were loaded with small amount of Pd by adding K_2PdCl_6 (0.027 mM) to the CMC−Fe^0 solution.[1,26] The amount of Pd used in this study was 0.1% (w/w) Fe. As determined in our prior study on starch-stabilized Fe nanoparticles,[6] the addition of a small fraction (0.1% w/w Fe) of Pd as a catalyst is able to increase reactivity by ~34 times based on the surface-area-normalized reaction rate constant. Because of the chainlike structure and macromolecular nature of CMC, the sorption of CMC should not prevent the accessibility of the CMC-stabilized core Fe particle for electron acceptors. Thus, once Pd^{2+} ions are added, they are reduced to Pd^0 by the Fe nanoparticles, resulting in Fe−Pd bimetallic nanoparticles. Direct evidence for the formation of microscale Fe−Pd bimetallic particles in the absence of a stabilizer has been reported by others.[27,28] In this study, the level of Pd was too low to be discernible from the transmission electron microscopy (TEM) images.

Physical Characterization. TEM micrographs were obtained using a Zeiss EM10 transmission electron microscope (Zeiss, Thornwood, NJ) following a previously reported procedure,[6] except that the preparation of the sample grids was carried out in an anaerobic glovebox fed with nitrogen gas.

Dynamic light scattering (DLS) tests were performed with a Nicomp 380 submicron particle sizer (PSS, Santa Barbara, CA) at a measurement angle of 90° (internal He−Ne laser, wavelength 633 nm). The DLS data were processed with the software package CW380 to yield the number-weighted size distributions. Solution viscosities were measured with a Gilmont falling-ball viscometer and then used to correct for the influence of viscosity on DLS measurements. In all measurements, triplicate samples of 0.1 g/L Fe were analyzed.

Fourier transform infrared (FTIR) spectroscopy measurements were carried out to explore the modes of interactions between CMC and the nanoparticle surface. The solution containing CMC-stabilized nanoparticles (1.0 g/L) was first centrifuged at high speed (9000*g*). Upon removal of the supernatant, the solid deposit was rinsed with DI water and then dried under a vacuum for 24 h. The dried sample was mixed with KBr to obtain KBr pellets consisting of 1.5% (w/w) of the nanoparticles. FTIR spectra of the CMC-stabilized nanoparticles were then recorded

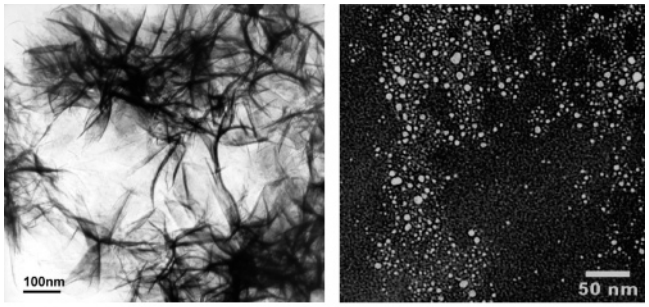

Figure 2. TEM images of 0.1 g/L freshly prepared (a) nonstabilized and (b) 0.2% (w/w) NaCMC-stabilized Fe−Pd nanoparticles.

using a Nicolet AVATAR 360 ESP spectrometer (Nicolet, Madison, WI). For comparison, FTIR spectra for CMC were obtained as a control.

Degradation of TCE. The TCE degradation effectiveness was tested in a series of duplicated batch experiments. The batch tests were carried out in 43-mL amber glass vials, filled with 43 mL of a solution containing a certain type of nanoscale particles (the headspace was set to nearly zero to minimize volatilization loss of TCE). TCE degradation was initiated by spiking 50 μL of a TCE stock solution (43 g/L TCE in methanol) into the solution containing the nanoparticles, which resulted in an initial TCE concentration of 50 mg/L. The bottles were capped with Teflon Mininert valves and mixed on a rotary shaker (40 rpm) placed in an incubator at 22 ± 1 °C. At selected time intervals, 0.1 mL of the aqueous sample, which included the suspended nanoparticles, was withdrawn using a 100-μL gastight syringe. Then, the sample was transferred into a 2-mL GC vial containing 1 mL of hexane for extraction of TCE. Upon phase separation, the extract was analyzed for TCE using an HP 6890 gas chromatograph equipped with an electron capture detector (ECD).

Analytical Methods. TCE was analyzed using an HP 6890 gas chromatograph equipped with an RTX-624 capillary column (Restek Co, Bellefonte, PA) and an ECD. The detailed procedures were described elsewhere.[6] Chloride was analyzed using a Dionex ion chromatograph (DX-120, Dionex, Sunnyvale, CA) equipped with an AS14 column, an AG14 guard column, and a 100-μL sample loop. Iron was analyzed with a flame atomic-absorption spectrophotometer (AAS) (220FS, Varian, Palo Alto, CA).

Results and Discussion

TEM, DLS, and UV−Vis Characterization of CMC-Stabilized Nanoparticles. Figure 2 compares the TEM images of the Fe−Pd nanoparticles prepared (a) in the absence of CMC and (b) in the presence of CMC. Figure 2a shows that, in the absence of the stabilizer, the freshly prepared Fe−Pd particles appeared as dendritic flocs rather than discrete particles. This type of aggregation was attributed to the magnetic and/or van der Waals forces between the Fe(0) particles.[29] In contrast, the fresh CMC-stabilized Fe−Pd particles shown in Figure 2b appeared as much finer nanoparticles with an average particle diameter (D) of 4.3 nm (standard deviation = 1.8 nm). In comparison, the starch-stabilized Fe−Pd nanoparticles had a mean size of 14.1 nm (standard deviation = 11.7 nm).[6] Both the smaller mean size and the narrower distribution of the CMC-stabilized particles indicate that CMC better suppressed the growth of the iron nanoparticles and maintained a higher surface area of the particles.

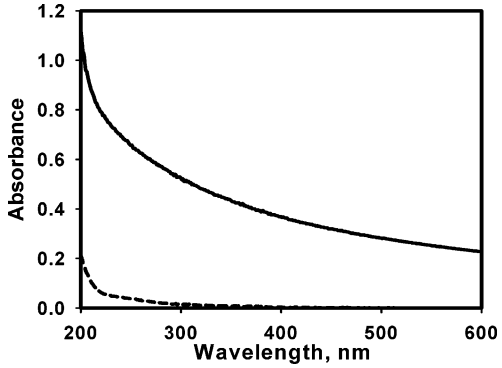

Figure 3. UV−vis absorption spectra of a solution containing 5 mg/L Fe(II) and 0.2% (w/w) NaCMC before (− − −) and after (−) reduction with $NaBH_4$.

The CMC-stabilized Fe−Pd nanoparticles exhibited superior stability against aggregation in water. Our observation revealed that, whereas nonstabilized particles precipitated in a few minutes, stabilized nanoparticles (0.1 g/L) remained fully dispersed in water until they were completely consumed by the water after 9 days of aging at room temperature.

Although TEM images provide direct visualization of the shape and morphology of nanoparticles, estimating the particle size from TEM images entails some key assumptions, including that (a) the particles are spherical, (b) the measured dried samples are the same as in the original solution, and (c) the population (i.e., number) of TEM samples is large enough and the selection of samples is representative. Clearly, deviations from each of the assumptions can result in significant errors. To facilitate a more accurate measurement of the particle size, DLS was employed to measure the size of the stabilized nanoparticles. Although the assumption of spherical shape is still needed, DLS offers some key advantages over TEM, including that (a) it measures the hydrodynamic size of particles in situ (i.e., in the original solution) and (b) it measures a much larger sample size (~0.5 mL/sample). The DLS data indicate that the fresh stabilized nanoparticles have a hydrodynamic size of 17.2 nm (standard deviation = 3.2 nm). Considering that the DLS and TEM measurements are naturally subjected to inherent sources of random and systematic error,[30] the TEM and DLS data appear to agree well.

Colloidal dispersions of metals typically exhibit absorption bands or broad regions of absorption in the ultraviolet−visible range.[31] Thus, the UV−vis absorption spectrum provides an instant indication of the formation of metal colloids. The pK_a value of CMC has been reported to be ~4.3,[25] and the pH of the CMC−Fe^{2+} solution (0.2% w/w CMC, 0.1 g/L Fe^{2+}) was measured to be ~6.1. Therefore, the carboxylic groups of CMC are expected to be almost fully disassociated and to interact strongly with the Fe^{2+} cations (Lewis acids). Upon reduction by $NaBH_4$, the solution color rapidly changed from clear to black, visually indicating the formation of Fe nanoparticles (pH after reduction ≈ 8.3). Accordingly, the absorbance intensity rose sharply, and the UV−vis spectrum displayed a monotonic and nearly exponential decaying profile as the wavelength increased (Figure 3). The exponential shape is characteristic of a bandlike electronic structure, which suggests that the reduced Fe exists not as isolated atoms, but rather as clusters.[6,31−33] Evidently, upon borohydride reduction, CMC-complexed Fe^{2+} ions are reduced to elemental Fe, which further undergoes nucleation and crystal growth,[12] resulting in the formation of the clustered Fe (i.e., the nanoparticles). In the meantime, however, the surface of the formed Fe nanoparticles reacts with

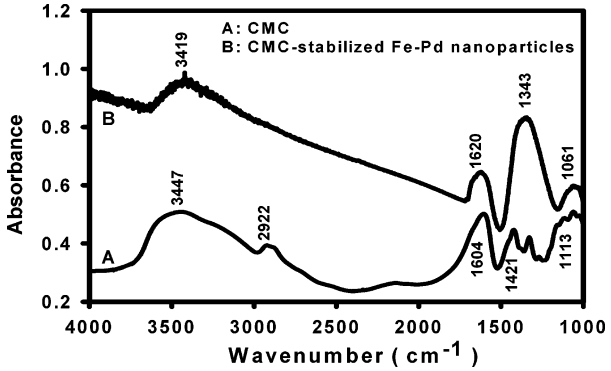

Figure 4. FTIR spectra of (A) CMC and (B) CMC-stabilized Fe−Pd nanoparticles.

Table 1. FTIR Peak Assignments for CMC and CMC-Stabilized Fe−Pd Nanoparticles[34]

peak position (cm^{-1})		
CMC alone	CMC-coated iron nanoparticles	assignment
3447	3419	O−H stretch
2922		asymmetric CH_2 stretch
1604	1620	COO^- (asymmetric)
1421	1343	COO^- (symmetric)
1113		C−O−C stretch (RCH_2OCH_2R)
1061	1061	C−O stretch (RCH_2OH)

water and interacts with CMC molecules, thereby preventing further particle growth.

FTIR Characterization of CMC-Coated Fe−Pd Nanoparticles and the Nature of Fe−CMC Interactions. To elucidate the stabilization mechanisms and to gain further insight into the interactions between the various functional groups of CMC and the nanoparticles, FTIR measurements were carried out on CMC and the CMC-stabilized nanoparticles. Figure 4 compares the characteristic stretching frequencies for CMC alone and for CMC-stabilized iron nanoparticles, and Table 1 gives the assignments of the peaks.[34] If CMC molecules are adsorbed to the surface of the iron nanoparticles, the stretching frequencies for the functional groups of CMC are expected to shift significantly.

Complexation between a carboxylate group and a metal such as Fe(0) can take place in four fashions: (I) monodentate chelating, (II) bidentate chelating, (III) bidentate bridging, and ionic interactions,[35,36] where the first three are illustrated in Figure 5. The separation of the symmetric and asymmetric stretches [$\Delta\nu = \Delta(\text{asym}) - \Delta(\text{sym})$] of the carboxylate group can be used to identify the bonding mechanism when compared to that of the corresponding carboxylate salt:[35,36] If $\Delta = 200-320\ cm^{-1}$, the binding is governed by monodentate interaction; if $\Delta < 110\ cm^{-1}$, the binding is governed by bidentate chelating interaction; and if $\Delta = 140-190\ cm^{-1}$, the binding is governed by bidentate bridging.

In the present work, $\Delta\nu$(adsorbed) was determined to be 277 cm^{-1} (1620 − 1343 cm^{-1}) from Figure 4. Thus, monodentate interaction is the primary mechanism for binding CMC molecules to Fe nanoparticles. The same type of interaction was also observed by Jones et al. during adsorption of polyacrylate onto hematite (α-Fe_2O_3).[37]

It is also noteworthy that the −OH stretching band shifts from 3447 cm^{-1} for CMC to 3419 cm^{-1} for the CMC−Fe particles. This observation indicates that an enhanced intermolecular hydrogen bond is formed between CMC and the Fe particle surface.[38,39] Given the abundance of −OH groups in CMC, this type of hydrogen bonding can be important in binding CMC to the Fe nanoparticles, although the individual bond strength might not be as strong as that between Fe and the carboxylate groups. This is in accordance with our prior observation that a water-soluble starch was able to stabilize the iron nanoparticles.[6] Because the starch contains no carboxymethyl groups, adsorption of starch molecules onto the nanoparticles is likely facilitated through this type of H-bonding.

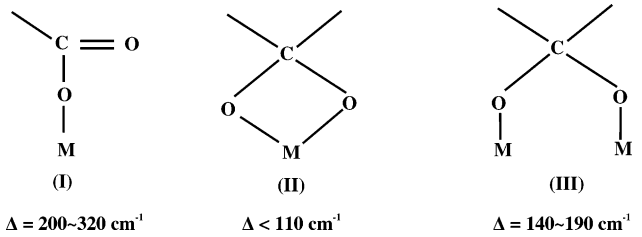

Figure 5. Modes of metal-carboxylate complexation: (I) monodentate chelating, (II) bidentate chelating, and (III) bidentate bridging. Δ is the separation between the symmetric and asymmetric stretches of the carboxylate group.

Judging from the FTIR results, it appears plausible that the stabilization of the clustered Fe nanoparticles is attributable to the adsorption of CMC molecules onto the surface of the nanoparticles. The adsorption process results in the encapsulation of the nanoparticles with a thin layer of negatively charged CMC. It is this protective CMC layer that suppresses the growth of the iron nanoparticles and prevents the particles from agglomeration through the electrostatic repulsion and/or steric hindrance between the CMC-coated nanoparticles.[40] In a recent study on the aggregation of agitate-coated nanoparticles,[41] researchers observed that electrostatic or DLVO interactions were the primary mechanism for particle stabilization/aggregation. Consequently, particle stabilization will be affected by the valence and concentration of cations. In the presence of NaCl, the researchers observed a critical coagulation concentration (CCC) of 180 mM (Na^+), below which there existed a strong electrostatic barrier that prevented the negatively charged nanoparticles from agglomerating. In our study, the total concentration of Na^+ in the nanoparticle suspension ranged from 8.2 to 61.4 mM, and no electrostatic destabilization of the CMC-stabilized nanoparticles was evident in all cases.

Reactivity of CMC-Stabilized Nanoparticles. The reactivity of the nanoparticles was investigated by testing the degradation of TCE. Figure 6 shows the TCE degradation rates obtained with various Fe−Pd particles. Considering that ethane is the primary final dechlorinated product,[42] the initial ration of Fe (0.1 g/L) to TCE was 1.17, i.e., Fe was initially in excess in the batch kinetic tests. It has been reported that pH is an important factor for iron nanoparticle reactivity.[43] Varying pH from 9 to 6 can increase reactivity by an order of magnitude. In the current study, the initial solution pH values for non-stabilized and CMC-stabilized Fe−Pd nanoparticle solution were ~6.8 and ~8.3 respectively. The pH change after TCE degradation reaction was <0.2 pH unit below the corresponding initial pH in both cases.

Assuming that TCE degradation in the initial stage (<40 min) follows pseudo-first-order reaction kinetics, the observed initial rate constant can be determined by fitting the experimental data to eq 1

$$-\frac{dC}{dt} = k_{obs}C = k_{SA}a_s\rho_m C \qquad (1)$$

where C is the TCE concentration (mg L^{-1}) at time t (h), k_{obs} is the observed pseudo-first-order rate constant, k_{SA} is the surface-area-based rate constant (L h^{-1} m^{-2}), a_s is the DLS-

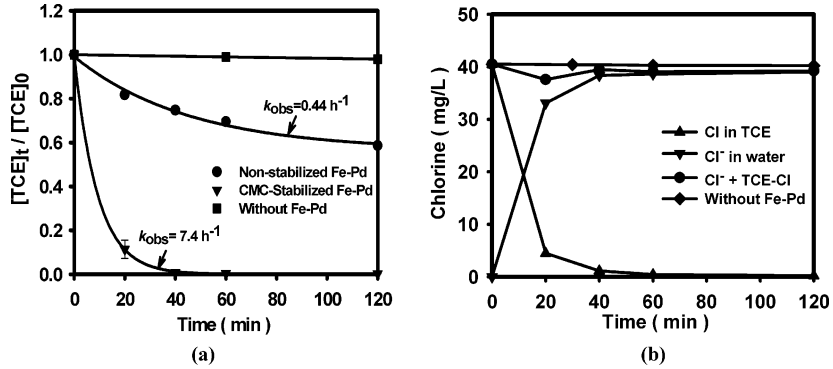

Figure 6. (a) Dechlorination of TCE using nonstabilized and CMC-stabilized Fe−Pd nanoparticles. (b) Evolution of chloride and TCE-Cl during dechlorination of TCE using CMC-stabilized Fe−Pd nanoparticles. [Initial TCE concentration, 50 mg L^{-1}; iron dose, 0.1 g L^{-1} as Fe; Pd/Fe ratio, 0.1/100 (w/w); NaCMC concentration, 0.2% (w/w)].

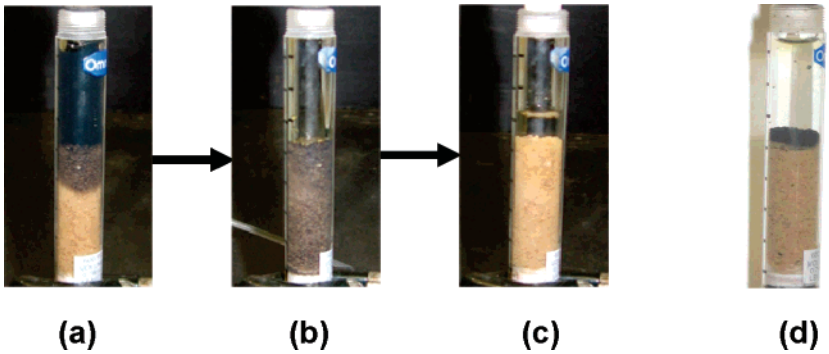

Figure 7. Transport of (a−c) CMC-stabilized Fe−Pd nanoparticles and (d) nonstabilized Fe−Pd aggregates through a loamy sand soil. The data were recorded as follows: (a) 0.5 min after one bed volume of a 1 g/L stabilized Fe−Pd suspension was gravity-fed to the soil bed, (b) after all of the suspension had passed through the bed, (c) after three bed volumes of DI water had passed through the bed shown in b, and (d) after one bed volume of 1 g/L nonstabilized Fe−Pd suspension had passed through the same soil bed.

based specific surface area of the nanoparticles (m^2 g^{-1}), and ρ_m is the mass concentration of the nanoparticles (g L^{-1}). Figure 6a shows that CMC stabilization enhanced the reactivity of the nanoparticles. When 0.2% CMC was added, the value of k_{obs} increased from 0.44 to 7.4 h^{-1} (a factor of 17). Nearly all of the TCE was destroyed within 40 min. Considering the pH difference between the solutions of nonstabilized and stabilized Fe−Pd nanoparticles, the reactivity difference between these two particles could be even greater. Compared to the starch-stabilized Fe−Pd nanoparticles,[6] the fresh CMC-stabilized nanoparticles offered a 2-times-greater k_{obs} value. The k_{SA} value for CMC-stabilized nanoparticles was 1.56 L $h^{-1}m^{-2}$ based on a DLS diameter of 17.2 nm.

It is well-known that TCE degradation entails a series of reaction steps and that toxic intermediates such as vinyl chloride (VC) and dichloroethenes (DCEs) must be eliminated rapidly, which justifies the pivotal importance of reaction kinetics in the environmental dechlorination processes. During the course of TCE degradation by CMC-stabilized Fe−Pd nanoparticles, halogenated intermediates, such as VC and *cis*- or *trans*-DCE, were not detected. Trace amounts (∼25 μg/L) of 1,1-DCE were detected in the initial stage of TCE degradation; however, it became nondetectable after 20 min. Figure 6b shows that the chloride production rate was nearly stoichiometrically coupled with the TCE degradation rate during the 2-h degradation of TCE using the CMC-stabilized Fe−Pd nanoparticles. (Note: The TCE remaining is reflected by the amount of Cl that remains associated with TCE, denoted as TCE-Cl.) The nearly perfect chlorine mass balance indicates the rapid and nearly complete dechlorination of TCE.

Soil Mobility of CMC-Stabilized Nanoparticles. As a preliminary test of the mobility of the CMC-stabilized and nonstabilized Fe−Pd nanoparticles in soil, simple column breakthrough and elution tests were carried out with a 2.7-mL loamy sand soil bed (obtained from Auburn, AL) packed in a glass column (1 cm i.d.). The salient soil properties are as follows: porosity, 0.35; hydraulic conductivity, 0.25 cm/min; sand content, 84%; silt content, 10%; clay content, 6%. In the tests, a 2.7-mL portion of a 1 g L^{-1} Fe−Pd suspension [either stabilized with 0.8% (w/w) CMC or nonstabilized] was gravity-fed onto the soil bed, and the eluent was collected at the bottom of the bed (Figure 7a). After ∼12 min, all of the suspension had passed through the column (Figure 7b). Then, approximately three bed volumes of deionized water were passed through the soil bed to elute the particles in the soil bed (Figure 7c). Figure 7 shows that, whereas the stabilized Fe−Pd nanoparticles were able to pass through and be completely dispersed in the soil bed, the nonstabilized Fe−Pd particles were retained on the top of the soil bed. When the exiting Fe−Pd suspension was collected and analyzed for Fe, ∼98% of the Fe introduced was recovered in the CMC-stabilized Fe−Pd suspension eluent, indicating that no nanoparticles were retained irreversibly. However, only ∼ 0.2% of the nonstabilized Fe was detected in approximately three bed volumes of the effluent water.

Conclusions

In summary, this study demonstrated that carboxymethyl cellulose can be used for effective stabilization of zerovalent iron nanoparticles to yield stable dispersions with sizes smaller than 17.2 nm. Compared to nonstabilized iron nanoparticle aggregates, the stabilized nanoparticles display greater reactivity for TCE dechlorination and are highly mobile in a sandy soil. This technology holds the promise to facilitate more effective

applications of Fe−Pd nanoparticles for in situ soil and groundwater remediation.

Acknowledgment

The authors thank Prof. R. B. Gupta for his assistance with DLS applications. This work was partially funded by a USEPA STAR grant (GR832373) and by a grant from the USGS-Alabama Water Resources Research Institute.

Literature Cited

(1) Wang, C. B.; Zhang, W. X. Synthesizing Nanoscale Iron Particles for Rapid and Complete Dechlorination of TCE and PCBs. *Environ. Sci. Technol.* **1997**, *31*, 2154.

(2) Gillham, R. W. Discussion of Nano-scale Iron for Dehalogenation. *Ground Water Monit. Remed.* **2003**, *23*, 6.

(3) Moran, T. *New Technology Revolutionizing Groundwater Clean-up; Nanoparticles are 1,000 Times Thinner Than Human Hair*; E-Wire Press Release, Lehigh University: Bethelehem, PA, Mar 13, 2002; http://www.ewire.com/display.cfm/Wire_ID/1017 (accessed Nov 2006).

(4) Mondal, K.; Jegadeesan, G.; Lalvani, S. B. Removal of Selenate by Fe and NiFe Nanosized Particles. *Ind. Eng. Chem. Res.* **2004**, *43*, 4922.

(5) Schrick, B.; Hydutsky, B. W.; Blough, J. L.; Mallouk, T. E. Delivery Vehicles for Zerovalent Metal Nanoparticles in Soil and Groundwater. *Chem. Mater.* **2004**, *16*, 2187.

(6) He, F.; Zhao, D. Preparation and Characterization of a New Class of Starch-Stabilized Bimetallic Nanoparticles for Degradation of Chlorinated Hydrocarbons in Water. *Environ. Sci. Technol.* **2005**, *39*, 3314.

(7) Glavee, G. N.; Klabunde, K. J.; Sorensen, C. M.; Hadjipanayis, G. C. Chemistry of Borohydride Reduction of Iron(II) and Iron(III) Ions in Aqueous and Nonaqueous Media. Formation of Nanoscale Fe, FeB, and Fe_2B Powders. *Inorg. Chem.* **1995**, *34*, 28.

(8) Li, F.; Vipulanandan, C.; Mohanty, K. K. Microemulsion and Solution Approaches to Nanoparticle Iron Production of Degradation of Trichloroethylene. *Colloids Surf. A* **2003**, *223*, 103.

(9) Suslick, K. S.; Fang, M.; Hyeon, T. Sonochemical Sythesis of Iron Colloids. *J. Am. Chem. Soc.* **1996**, *118*, 11960.

(10) Khalil, H.; Mahajan, D.; Rafailovich, M.; Gelfer, M.; Pandya, K. Synthesis of Zerovalent Nanophase Metal Particles Stabilized with Poly-(ethylene glycol). *Langmuir* **2004**, *20*, 6896.

(11) Wonterghem, J. V.; Morup, S.; Charles, S. W.; Wells, S.; Villadsen, J. Formation of a Metallic Glass by Thermal Decomposition of $Fe(CO)_5$. *Phys. Rev. Lett.* **1985**, *55*, 410.

(12) Cushing, B. L.; Kolesnichenko, V. L.; O'Connor, C. J. Recent Advances in the Liquid-Phase Syntheses of Inorganic Nanoparticles. *Chem. Rev.* **2004**, *104*, 3893.

(13) Kataby, G.; Prozorov, T.; Koltypin, Y.; Cohen, H.; Sukenik, C. N.; Ulman, A.; Gedanken, A. Self-Assembled Monolayer Coatings on Amorphous Iron and Iron Oxide Nanoparticles: Thermal Stability and Chemical Reactivity Studies. *Langmuir* **1997**, *13*, 6151.

(14) Kataby, G.; Cojocaru, M.; Prozorov, R.; Gedanken, A. Coating Carboxylic Acids on Amorphous Iron Nanoparticles. *Langmuir* **1999**, *15*, 1703.

(15) Sun, S.; Zeng, H. Size-Controlled Synthesis of Magnetite Nanoparticles. *J. Am. Chem. Soc.* **2002**, *124*, 8204.

(16) Kim, D. K.; Mikhaylova, M.; Zhang, Y.; Muhammed, M. Protective Coating of Superparamagnetic Iron Oxide Nanoparticles. *Chem. Mater.* **2003**, *15*, 1617.

(17) Si, S.; Kotal, A.; Mandal, T.; Giri, S.; Nakamura, H.; Kohara, T. Size-Controlled Synthesis of Magnetite Nanoparitcles in the Presence of Polyelectrolytes. *Chem. Mater.* **2004**, *16*, 3489.

(18) Ditsch, A.; Laibinis, P. E.; Wang, D. I. C.; Hatton, T. A. Controlled Clustering and Enhanced Stability of Polymer-Coated Magnetic Nanoparticles. *Langmuir* **2005**, *21*, 6006.

(19) Khalil, H.; Mahajan, D.; Rafailovich, M.; Gelfer, M.; Pandya, K. Synthesis of Zerovalent Nanophase Metal Particles Stabilized with Poly-(ethylene glycol). *Langmuir* **2004**, *20*, 6896.

(20) Ponder, S. M.; Darab, J. G.; Mallouk, T. E. Remediation of Cr(VI) and Pb(II) Aqueous Solutions Using Supported, Nanoscale Zero-valent Iron. *Environ. Sci. Technol.* **2000**, *34*, 2564.

(21) Ponder, S. M.; Darab, J. G.; Bucher, J.; Caulder, D.; Craig, I.; Davis, L.; Edelstein, N.; Lukens, W.; Nitsche, H.; Rao, L.; Shuh, D. K.; Mallouk, T. E. Surface Chemistry and Electrochemistry of Supported Zerovalent Iron Nanoparticles in the Remediation of Aqueous Metal Contaminants. *Chem. Mater.* **2001**, *13*, 479.

(22) Saleh, N.; Phenrat, T.; Sirk, K.; Dufour, B.; Ok, J.; Sarbu, T.; Matyjaszewski, K.; Tilton, R. D.; Lowry, G. V. Adsorbed Triblock Copolymers Deliver Reactive Iron Nanoparticles to the Oil/Water Interface. *Nano Lett.* **2005**, *5*, 2489.

(23) Sun, Y. P.; Zhang, W. X. Dispersion of Zero-Valent Iron Nanoparticles. In *Abstracts of Papers IEC-090, 229th ACS National Meeting, March 13−17, 2005*; American Chemical Society: San Diego, CA, 2005.

(24) Gilbert, R. D. *Cellulosic Polymers, Blends, and Composites*; Hanser/Gardner Publications: Cincinnati, OH, 1994.

(25) Magdassi, S.; Bassa, A.; Vinetsky, Y.; Kamyshny, A. Silver Nanoparticles as Pigments for Water-Based Ink-Jet Inks. *Chem. Mater.* **2003**, *15*, 2208.

(26) Grittini, C.; Malcomson, M.; Fernando, Q.; Korte, N. Rapid Dechlorination of Polychlorinated Biphenyls on the Surface of a Pd/Fe Bimetallic System. *Environ. Sci. Technol.* **1995**, *29*, 2898.

(27) Doong, R. A.; Lai, Y. J. Dechlorination of Tetrachloroethylene by Palladized Iron in the Presence of Humic Acid. *Water Res.* **2005**, *39*, 2309.

(28) Jovanovic, G. N.; Plazl, P. Z.; Sakrittichai, P.; Al-Khaldi, K. Dechlorination of *p*-Chlorophenol in a Microreactor with Bimetallic Pd/Fe Catalyst. *Ind. Eng. Chem. Res.* **2005**, *44*, 5099.

(29) Zhang, L.; Manthiram, A. Chains Composed of Nanosize Metal Particles and Identifying the Factors Driving Their Formation. *Appl. Phys. Lett.* **1997**, *70*, 2469.

(30) Zheng, J.; Stevenson, M. S.; Hikida, R. S.; Van Patten, P. G. Influence of pH on Dendrimer-Protected Nanoparticles. *J. Phys. Chem. B* **2002**, *106*, 1252.

(31) Creighton, J. A.; Eadon, D. G. Ultraviolet-Visible Absorption Spectra of the Colloidal Metallic Elements. *J. Chem. Soc., Faraday Trans.* **1991**, *87*, 3881.

(32) Kreibig, U.; Vollmer, M. *Optical Properties of Metal Clusters*; Spring-Verlag: Berlin, 1995.

(33) Zhao, M.; Sun, L.; Crooks, R. M. Preparation of Cu Nanoclusters within Dendrimer Templates. *J. Am. Chem. Soc.* **1998**, *120*, 4877.

(34) Brown, D. W.; Floyd, A. J.; Sainsbury, M. *Organic Spectroscopy*; John Wiley & Sons: Bath, U.K., 1988.

(35) Deacon, G. B.; Phillips, R. J. Relationship between the Carbon−Oxygen Stretching Frequencies of Carboxylate Complexes and the Type of Carboxylate Coordination. *Coord. Chem. Rev.* **1980**, *33*, 227.

(36) Wu, N.; Fu, L.; Su, M.; Aslam, M.; Wong, K. C.; Dravid, V. P. Interaction of Fatty Acid Monolayers with Cobalt Nanoparticles. *Nano Lett.* **2004**, *4*, 383.

(37) Jones, F.; Farrow, J. B.; Bronswijk, W. V. An Infrared Study of a Polyacrylate Flocculant Adsorbed on Hematite. *Langmuir* **1998**, *14*, 6512.

(38) Sylvestre, J. P.; Poulin, S.; Kabashin, A. V.; Sacher, E.; Meunier, M.; Luong, J. H. T. Surface Chemistry of Gold Nanoparticles Produced by Laser Ablation in Aqueous Media. *J. Phys. Chem. B* **2004**, *108*, 16864.

(39) Bellamy, L. J. *The Infrared Spectra of Complex Molecules*; Chapman and Hall: London, 1975.

(40) O'Melia, C. R. In *Physicochemical Processes for Water Quality Control*; Weber, W. J., Jr., Ed.; Wiley: New York, 1972.

(41) Chen, K. L.; Mylon, S. E.; Elimelech, M. Aggregation Kinetics of Alginate-Coated Hematite Nanoparticles in Monovalent and Divalent Electrolytes. *Environ. Sci. Technol.* **2006**, *40*, 1516.

(42) Liu, Y.; Majetich, S. A.; Tilton, R. D.; Sholl, D. S.; Lowry, G. V. TCE Dechlorination Rates, Pathways, and Efficiency of Nanoscale Iron Particles with Different Properties. *Environ. Sci. Technol.* **2005**, *39*, 1338.

(43) Song, H.; Carraway, E. R. Reduction of Chlorinated Ethanes by Nanosized Zero-Valent Iron: Kinetics, Pathways, and Effects of Reaction Conditions. *Environ. Sci. Technol.* **2005**, *39*, 6237.

Received for review August 17, 2006
Revised manuscript received October 16, 2006
Accepted October 18, 2006

IE0610896